Electronic Supplementary Material (ESI) for Journal of Materials Chemistry A.

Supporting Information

Mxene–modulated 3D crosslinking network of hierarchical flower–like MOF derivatives towards ultra–efficient microwave absorption property

Hui-Ya Wang, Xiao-bo Sun, Guang-Sheng Wang*

XPS was applied to further clarify the state bonding between CO (CN_1O) and $Ti_3C_2T_x$ MXene. As shown in Fig. S4a, the high resolution XPS of Ti 2p spectrum can be fitted into four main peaks corresponding to the Ti-C, Ti^{2+}, Ti^{3+}, and Ti-O, respectively. Compared with $Ti_3C_2T_x$ MXene, the percentage of Ti-O bond increases in the COT and CN_1OT composites, whereas no diffraction peak can be assigned to TiO_2 in XRD pattern. It implies CO (CN_1O) can be successfully grown on the surface of $Ti_3C_2T_x$ MXene via strong covalent bond interaction (O–C=O, Ti-O) rather than simply physical contact. This can be further evidenced by Ti 2p peaks of COT and CN_1OT composites migrate to lower regions of binding energy in contrast with $Ti_3C_2T_x$ MXene.[1] For COT and CN_1OT, the high-resolution XPS spectrums (Fig. S4b) reveal Co 2p is composed of the characteristic spin orbits of Co^{2+} and Co^{3+} and two satellite peaks, indicating that Co has +2 and +3 oxidation states. As displayed in Fig. S4c, the fitting peaks at 854.6 and 871.8 eV belong to Ni^{2+}, while the peaks at 856.6 and 873.7 eV are assigned to Ni^{3+}. Two remaining peaks at 861.5 and 878.8 eV 8 are related to satellite peaks of Ni $2p_{3/2}$ and Ni $2p_{1/2}$, respectively.[2]

References

1. R. Zhang, Z. Xue, J. Qin, M. Sawangphruk, X. Zhang, R. Liu, J. Energy Chem., 2020, **50**, 143–153.
2. H. Hu, J. Liu, Z. Xu, L. Zhang, B. Cheng, W. Ho, Appl. Surf. Sci., 2019, **478**, 981–990.

Table S1 Zeta potentials of as-prepared samples.

Sample	Zeta potential (mV)
$Ti_3C_2T_x$	-30.7
CM	25.9
CN_1M	47.3
CN_5M	33.5
CN_9M	29.8
CMT	-2.5
CN_1MT	-0.8
CN_5MT	-12.0
CN_9MT	-11.3

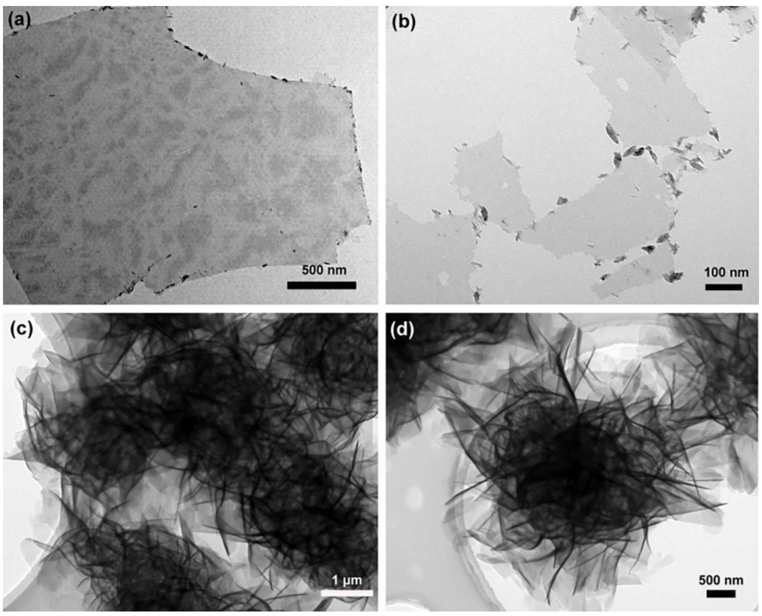

Fig. S1 TEM image of (a,b) $Ti_3C_2T_x$ nanosheets and (c,d) CM flowers.

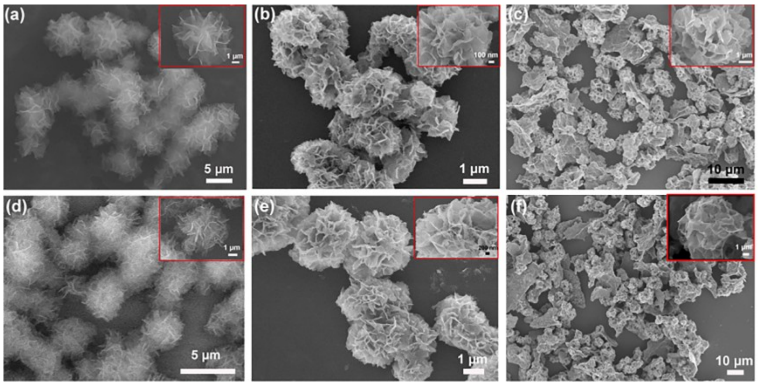

Fig. S2 SEM image of various samples, (a) CM, (b) CO, (c) COT, (d) CN_1M, (e) CN_1O, (f) CN_1OT.

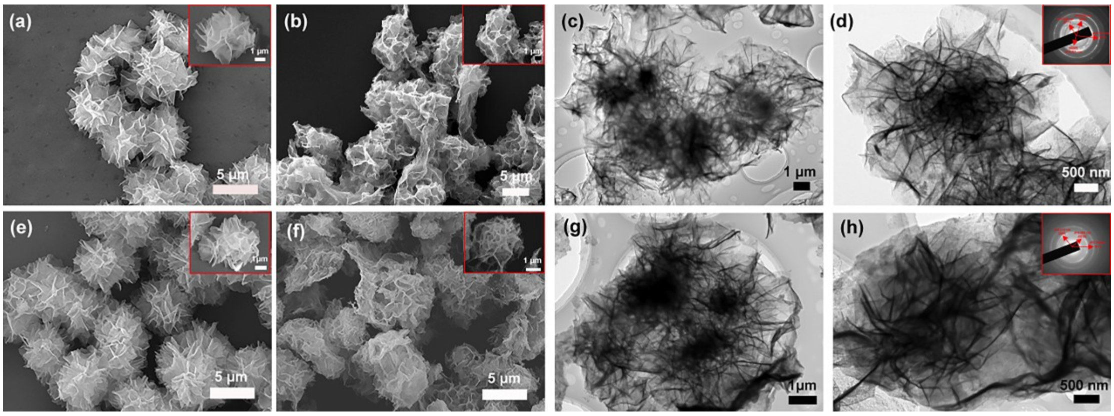

Fig. S3 SEM images of (a) CN_5M, (b) CN_5OT, (e) CN_9M and (f) CN_9OT composites, TEM images of (c,d) CN_5OT and (g,h) CN_9OT.

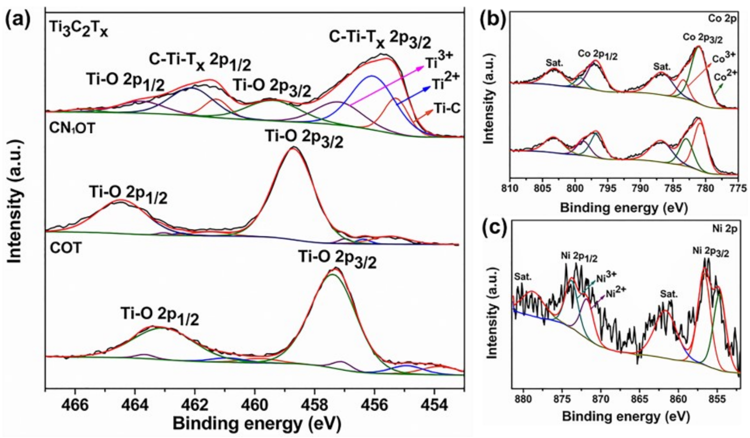

Fig. S4 High-resolution XPS spectra of (a) Ti 2p, (b) Co 2p and (c) Ni 2p of $Ti_3C_2T_x$, COT and CN_1OT.

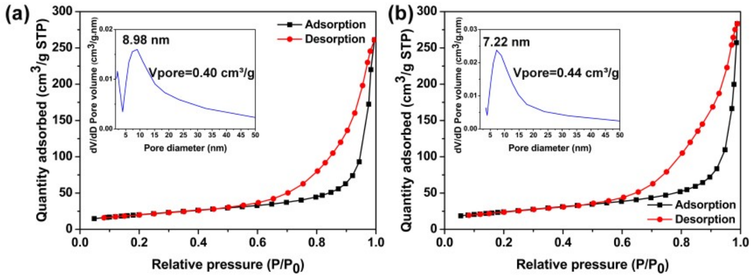

Fig. S5 N_2 adsorption-desorption isotherm and pore size distribution of (a) CO and (b) CN_1O composites, respectively.

Table S2 The element content of Co and Ni in different CNO samples by ICP analysis.

Sample	CN_1O	CN_5O	CN_9O
Co	794.8	545.2	564.0
Ni	32.18	190.1	324.2
Co:Ni	24.7:1	2.87:1	1.74:1

Fig. S6 Images of CN_1OT composites on (a dandelion and (b) flower plates.

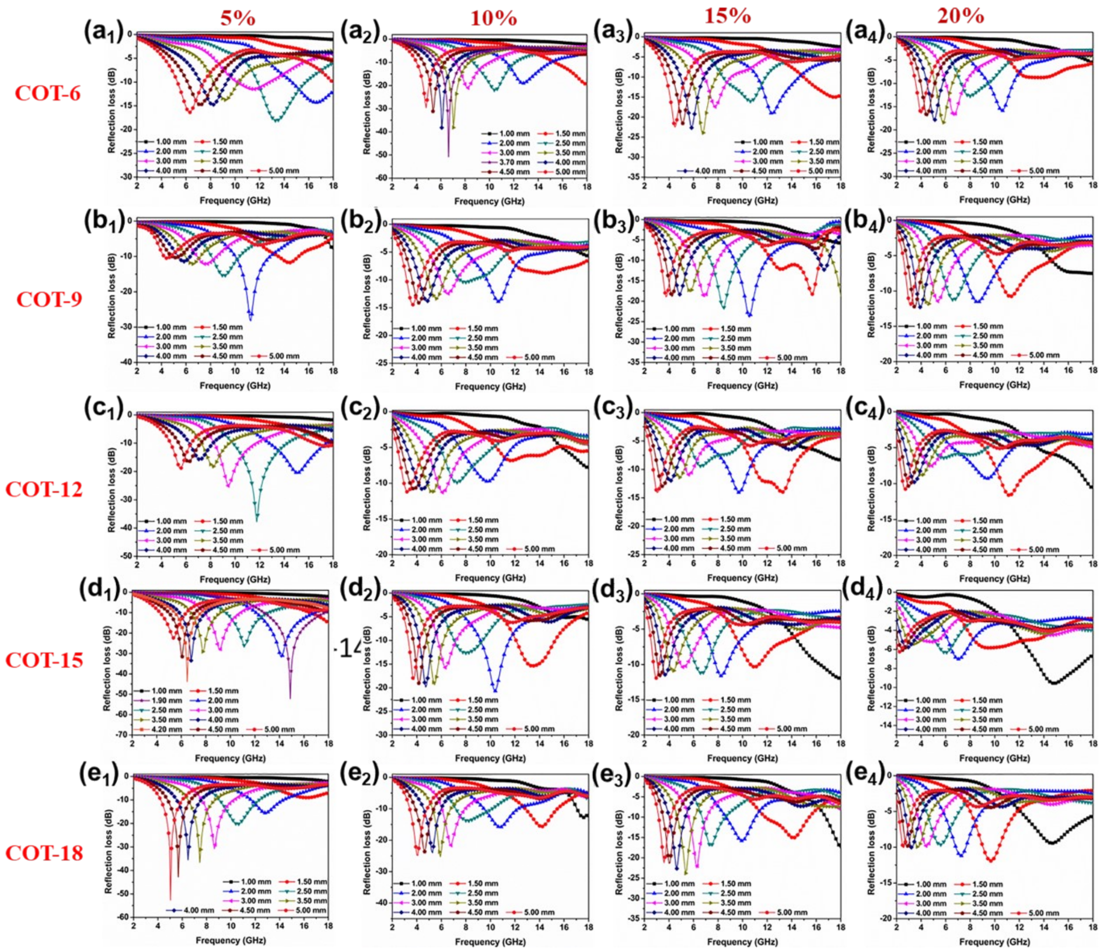

Fig. S7 2D RL curves of the COT-x series.

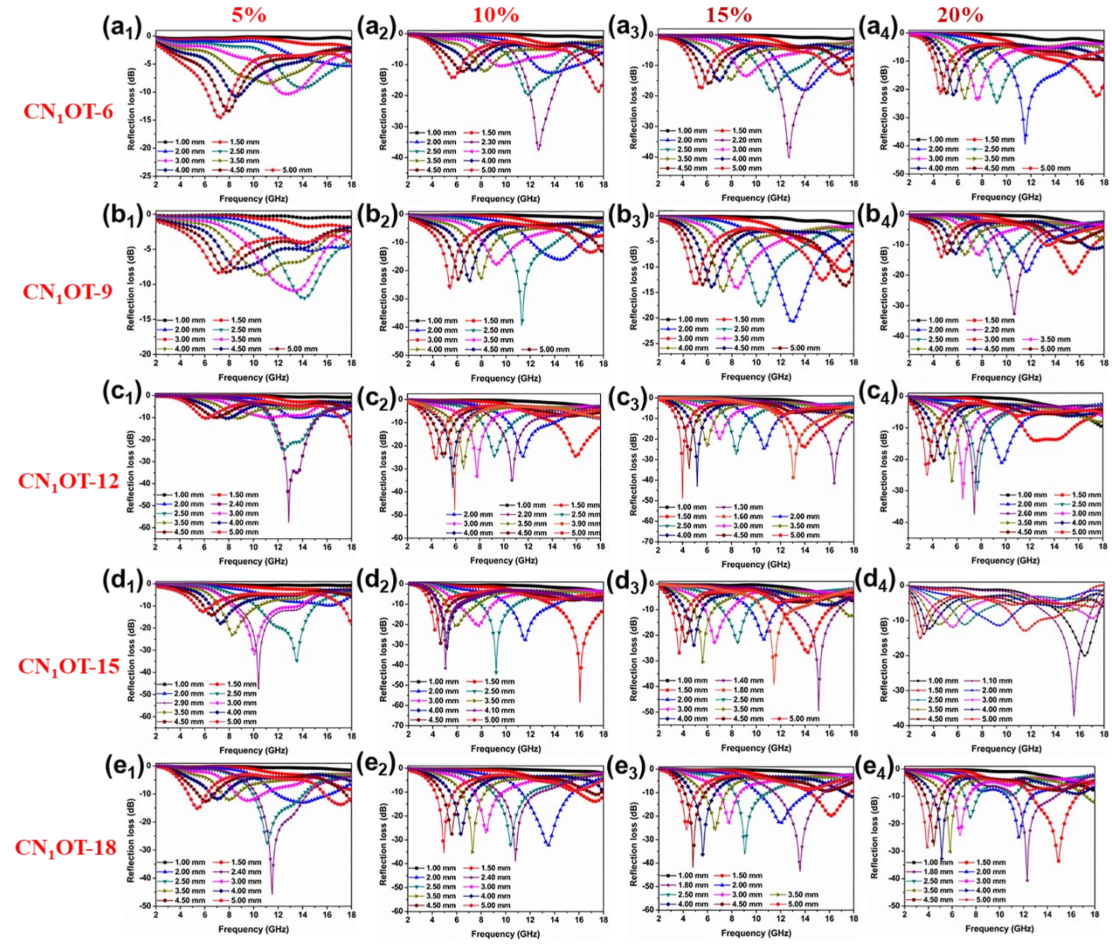

Fig. S8 **2**D RL curves of the CN_1OT-x series

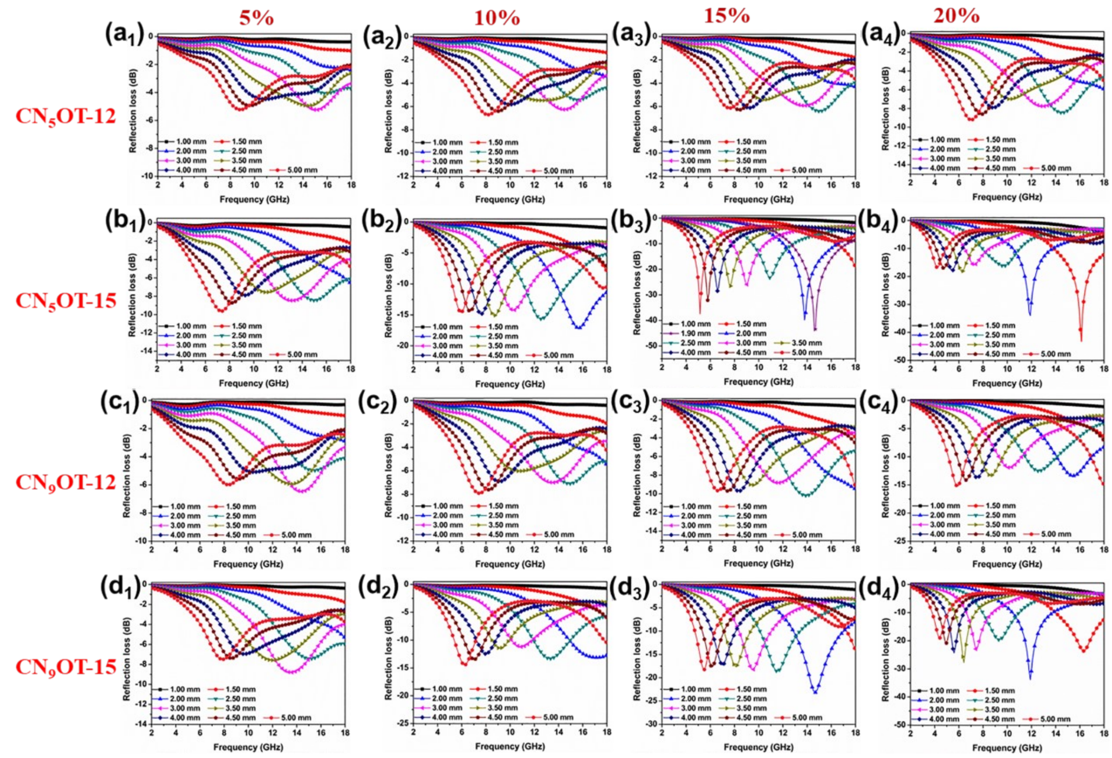

Fig. S9 **2**D RL curves of the CN_5OT-x and CN_9OT-x series

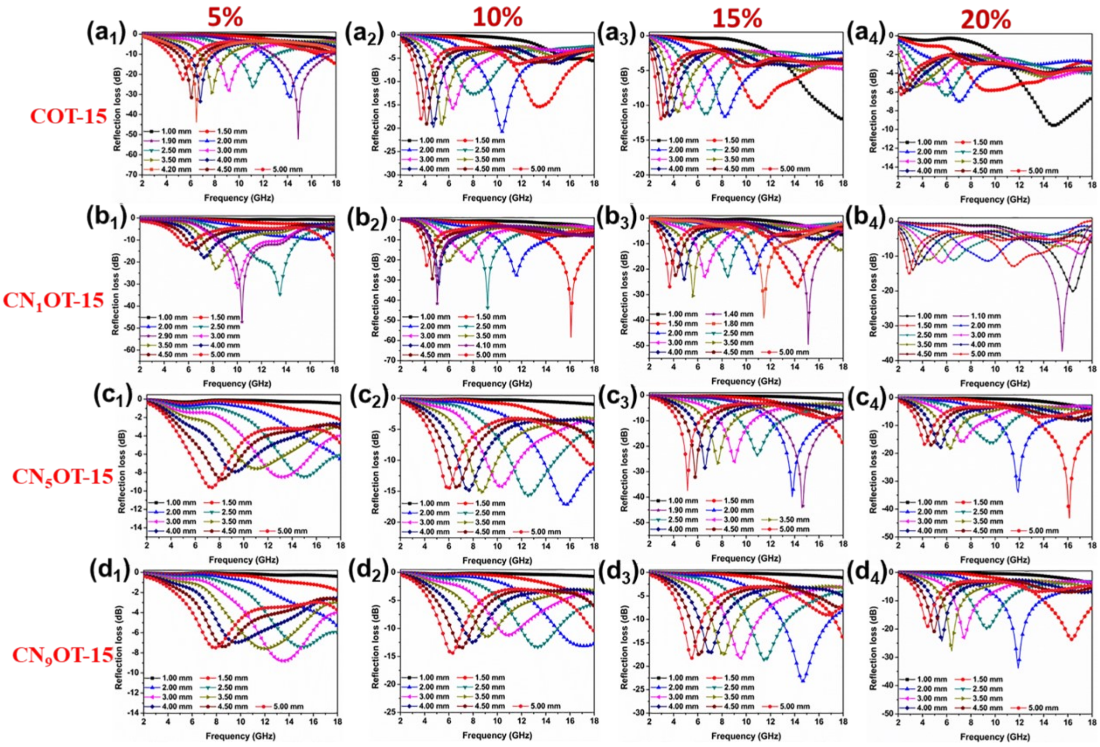

Fig. S10 2D RL curves of the COT and CNOT-x series.

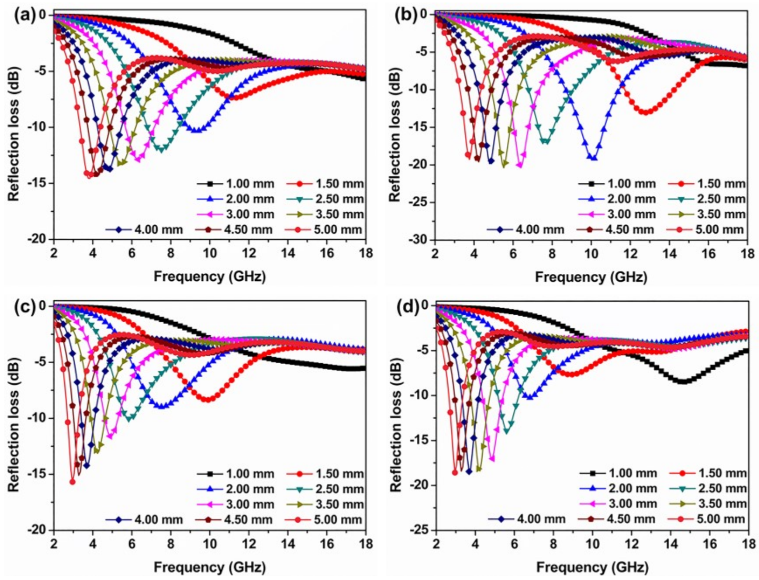

Fig. S11 2D RL curves of pure MXene with different filler content in PVDF, (a) 5 wt%, (b) 10wt%, (c) 15wt% and (d) 20wt%.

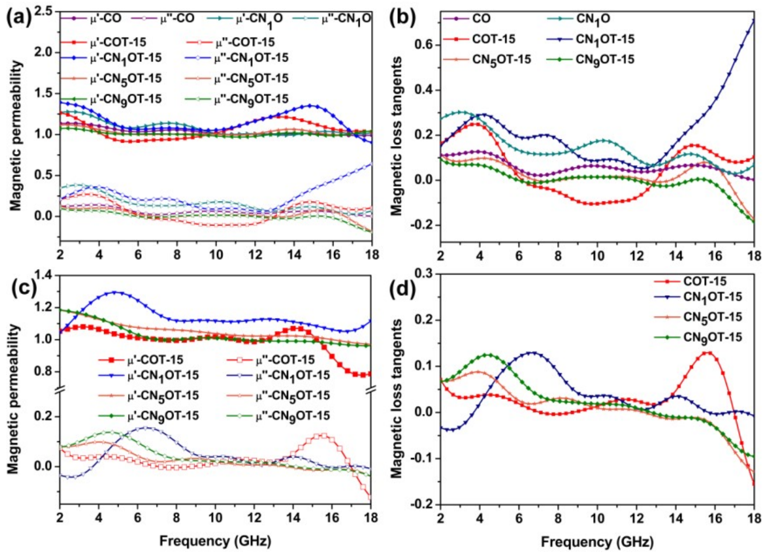

Fig. S12 Frequency dependence of electromagnetic parameters for various composites, (a) complex permeability and (b) magnetic loss tangent of samples with 20 wt% loading, permeability of (c) CN_1OT–x with 10 wt% filler content and (d) CN_1OT–15 with different filler loading.

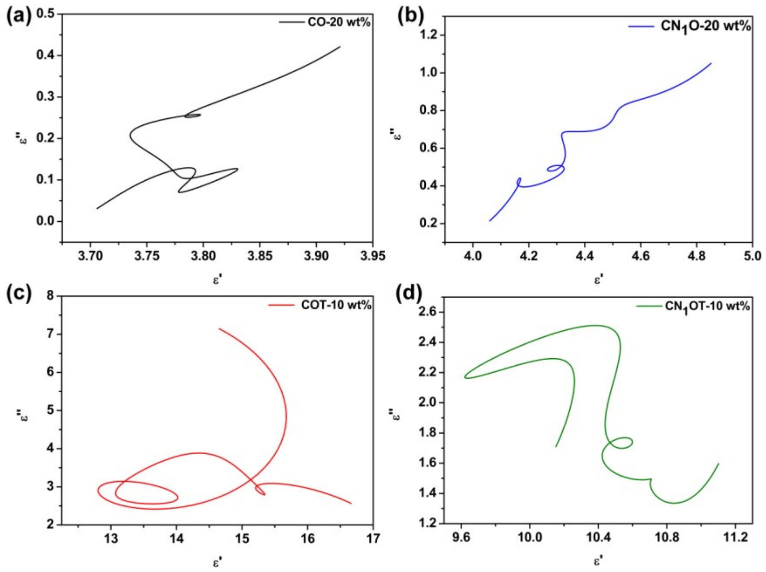

Fig. S13 The relationship between real and imaginary part of permittivity for various samples, (a) CO and CN_1O with filler content of 20 wt%, (c) COT and CN_1OT composites with 10 wt% filler loading.